Observation of strain in pseudomorphic $Si_{1-x}Ge_x$ by tracking phonon participation in Si/SiGe resonant interband tunnel diodes via electron tunneling spectroscopy

Ronghua Yu,[1] R. Anisha,[2] Niu Jin,[2] Sung-Yong Chung,[2] Paul R. Berger,[1,2,a)] Thomas J. Gramila,[1] and Phillip E. Thompson[3]
[1]Department of Physics, The Ohio State University, Columbus, Ohio 43210, USA
[2]Department of Electrical and Computer Engineering, The Ohio State University, Columbus, Ohio 43210, USA
[3]Naval Research Laboratory, Washington, DC 20375, USA

(Received 21 February 2009; accepted 29 June 2009; published online 10 August 2009)

High-sensitivity and low-noise electron tunneling spectroscopy was used to measure the phonon spectra via band-to-band tunneling in Si/SiGe resonant interband tunneling diodes (RITD), tracking the effects of the weighted average Ge percentage in the central tunneling spacer. With a composite RITD tunneling barrier consisting of 4 nm of intrinsic $Si_{0.60}Ge_{0.40}$ and n nm of intrinsic Si ($n=4,6,8,10$) all grown on Si substrates, the transverse acoustic (TA) phonon of $Si_{0.60}Ge_{0.40}$ was identified and the energy was measured to be 16 ± 1 meV. This is higher than the ~14 meV energy of the TA phonon in $Si_{0.60}Ge_{0.40}$ reported from measurements of Esaki tunnel diodes fabricated from bulk single crystals. The increase is attributed to the compressive strain in the $Si_{0.60}Ge_{0.40}$ layer grown on Si substrates. The observation of the upshift of phonon energy with strain by electron tunneling spectroscopy demonstrates the capability of electron tunneling spectroscopy to characterize residual strain. © *2009 American Institute of Physics*. [DOI: 10.1063/1.3187832]

I. INTRODUCTION

Negative differential resistance (NDR) devices cointegrated with conventional Si transistor technology [metal-oxide-semiconductor field effect transistors (MOSFETs) or SiGe heterojunction bipolar transistors] provide a pathway for efficient circuits.[1–4] Compared to their all-transistor counterparts, the combination of suitable tunnel diodes with transistors utilizes, in general, fewer devices, less chip area, and reduced power consumption for the same functionality. This is one thrust perceived by the International Technology Roadmap for Semiconductors (ITRS) to mitigate pressures to achieve aggressively scaled complementary MOS.[5] Two of the more promising circuit applications enhanced by tunnel diodes are dense embedded memory and mixed signal circuits, which have significantly different current density requirements. A low-power tunneling static random access memory cell[1] prefers low current for low-power consumption, but one which is high enough to charge up the interconnect lines for reasonable switching times. A voltage-controlled oscillator[4] requires high current for the generation of strong microwave signals. Past Si/SiGe resonant interband tunnel diode (RITD) work has explored this broad current range by varying the tunneling spacer thickness[6–12] and the Ge percentage.[8] Increased Ge percentage in the RITD spacer manifests as an elevated current density commonly attributed to the lowering of the barrier from the reduced bandgap.[13] This experiment was designed to track the phonon participation in band-to-band tunneling across the composite RITD tunneling spacer, including compressive strain in the SiGe and tensile strain in the adjacent Si. In addition, the ability to infer the residual strain energy in pseudomorphic SiGe was also facilitated.

The determination of residual strain is important because strained Si and $Si_{1-x}Ge_x$ alloys are in the process of replacing conventional Si in the MOSFET channel as these devices scale to deep submicron dimensions because of the improved mobilities under strain.[14–16] Pseudomorphic tensile biaxially strained Si can be grown on relaxed $Si_{1-x}Ge_x$ virtual substrates formed by growing compositionally graded $Si_{1-x}Ge_x$ buffer layers on Si substrates. Compressive biaxially strained $Si_{1-y}Ge_y$ can be grown on Si or $Si_{1-x}Ge_x$ virtual substrates for $y>x$, as the lattice constant of $Si_{1-x}Ge_x$ increases with increasing Ge content x. The amount of electron or hole mobility improvement depends on the degree of residual strain present. Further, the strain fields are nonuniform over the nanoscale channel depths and shared between Si and SiGe across the interface, adjacent the active channel. Therefore, a direct measurement of this residual strain experienced by the carriers is important for a complete understanding of MOSFETs with strained Si and $Si_{1-x}Ge_x$ channels or recessed source/drain regions to facilitate subsequent device optimization.

Unfortunately, present techniques to measure residual strain in scaled devices are not suitable. X-ray diffraction (XRD)[17–19] is less useful in this regime, as the selectively deposited SiGe regions can be extremely small, rendering them undetectable by the XRD technique. While transmission electron microscopy (TEM) could determine the morphology and therefore strain, at the nanoscale, cross-sectional TEM is a destructive test, requiring abrasive TEM sample preparation that can sometimes cause pseudomorphic

a)Electronic mail: pberger@ieee.org.

 © 2009 American Institute of Physics

Downloaded 10 Aug 2009 to 164.107.166.49. Redistribution subject to AIP license or copyright; see http://jap.aip.org/jap/copyright.jsp

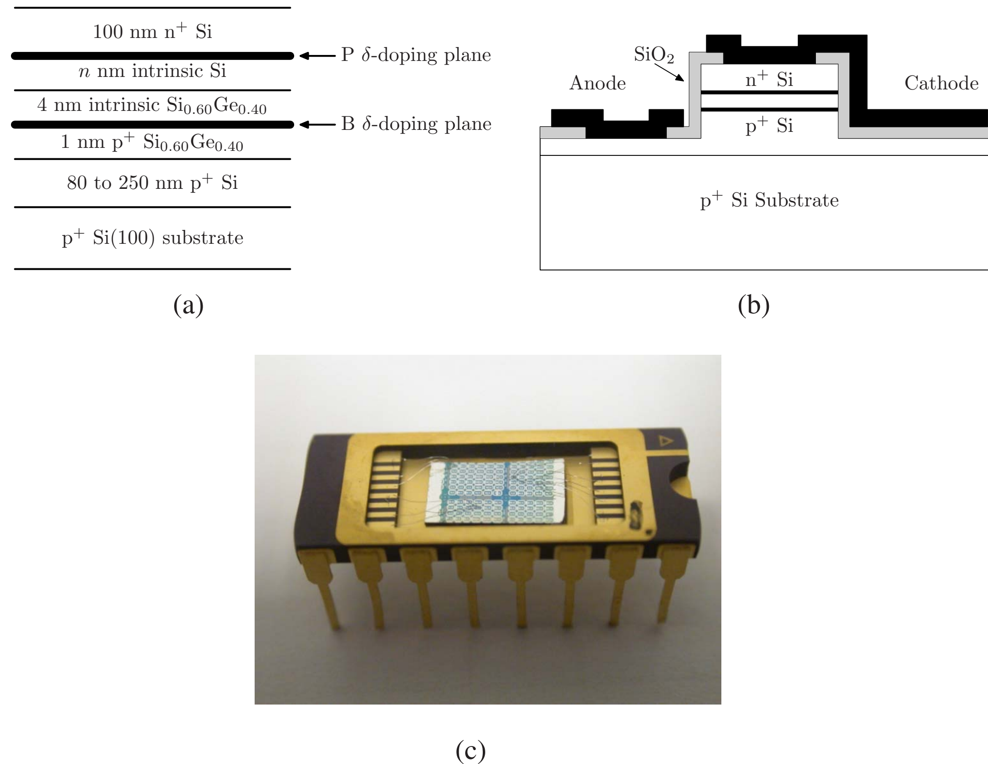

FIG. 1. (Color online) (a) The structures of the Si/SiGe RITDs, referred to as $-1/4/n$ structures with $n=4,6,8,10$, incorporating a 4 nm $Si_{0.60}Ge_{0.40}$ layer and a n nm Si layer in the composite tunneling barrier. (b) The cross section of a Si/SiGe RITD with two bonding pads. The gray areas are SiO_2, and the black areas are contact metal. (c) A photograph of a completed device following packaging and wire bonding.

films to partially relax. The strain in $Si_{1-x}Ge_x$ films could be determined from the locations of the three peaks in the Raman spectra related to the vibrational modes of the nearest neighbor Ge–Ge, Si–Ge, and Si–Si pairs in the alloys[20–22] but this technique requires optical access to the region of interest and the amount of residual strain may vary across the film's depth.

The lattice constant of bulk, or fully relaxed, $Si_{1-x}Ge_x$ alloy is a function of its composition x. However, the residual strain in a pseudomorphic $Si_{1-y}Ge_y$ film grown on a lattice-mismatched substrate (e.g., Si or a relaxed $Si_{1-x}Ge_x$ virtual substrate with $y \neq x$) depends on the composition of the film, the percentage of film relaxation, and also the composition of the substrate. The film relaxation is also a function of the thermal cycling experienced by the wafer and therefore is not solely determined by the lattice constant misfit alone. Thus, a direct measurement is needed to track this residual film strain with the mobility enhancements.

As a result of the change in lattice parameters as compared to the bulk, strain can alter the phonon spectra in $Si_{1-x}Ge_x$ alloy films. As Si, Ge, and $Si_{1-x}Ge_x$ are all indirect semiconductors, electron tunneling spectroscopy, which measures the energy of the phonons participating in the tunneling process, can detect and characterize this strain by the shift of the phonon energies from their corresponding bulk or unstrained values. If these results were combined with predictive modeling, then a clear guide could be created to discern nanoscopic changes. In the electron tunneling experiment, the current-voltage (I-V) characteristic of the tunneling junction is measured at low temperature, typically 4.2 K, to suppress the thermal broadening effect. The small inflections in the I-V curve, due to the onset of participation of certain phonons in the tunneling process, are made more obvious by taking the derivatives, especially the second-order derivative.[23,24] The second-order derivative of the current with respect to the voltage,[24] d^2I/dV^2 versus V plot shows peaks corresponding to the various phonons participating in the tunneling process. These peak locations correspond to the energies of the phonons.

The transverse acoustic (TA), longitudinal acoustic (LA), longitudinal optical (LO), and transverse optical (TO) phonon energies of Si and Ge have been measured by Chynoweth *et al.*[24] and Payne,[25] while those of the $Si_{1-x}Ge_x$ alloys of various compositions were measured by Logan *et al.*[26] It should be noted that all these previous measurements used bulk materials only; therefore, the measured phonon energies were of unstrained materials and their crystal orientations were often not documented. In this article, we report the observation of strain in $Si_{1-x}Ge_x$ by electron tunneling spectroscopy using a Si/SiGe RITD structure, which indicates that electron tunneling spectroscopy is a potential technique for characterizing strain as well as tracking phonon participation in band-to-band tunneling.

II. EXPERIMENT

A. Sample design and fabrication

The tunneling structures used in this experiment are Si/SiGe RITDs, shown in Fig. 1(a), following previous reported RITD structures.[8,10] The intrinsic RITD structures in-

Downloaded 10 Aug 2009 to 164.107.166.49. Redistribution subject to AIP license or copyright; see http://jap.aip.org/jap/copyright.jsp

clude two δ-doping layers of opposite doping type with a composite tunneling barrier in between. The δ-doping layers essentially define the quantum wells for resonant interband tunneling. The tunneling barrier between the two δ-doping layers consists of 4 nm intrinsic $Si_{0.60}Ge_{0.40}$ and n nm intrinsic Si with $n=4,6,8,10$, hereafter referred to as $-1/4/4$, $-1/4/6$, $-1/4/8$, and $-1/4/10$ structures, respectively (the "-1" refers to the 1 nm SiGe layer grown prior to the deposition of the B δ-doped layer, employed to inhibit the B diffusion[10]). The total tunneling spacer thicknesses were chosen to lower the absolute current densities, which if too high would cause both Ohmic losses that would shift the phonon energies and potentially lead to significant Joule heating during low-temperature measurements, thereby broadening the measured phonon peaks. A constant thickness of 4 nm was chosen for the $Si_{0.60}Ge_{0.40}$ layer so that it would remain below the critical thickness.[27]

The design of the tunneling structures for this experiment is based on the authors' past work developing Si/SiGe-based tunnel diodes for circuit applications.[6–12] The peak-to-valley current ratio (PVCR) and peak current density (PCD) are two major figures of merit characterizing a tunnel diode's electrical performance. Both are determined by the tunneling process in the diode structure along with secondary effects. One such secondary effect is the excess current, which originates from tunneling through defect states within the forbidden semiconductor energy bandgap. In general, for many circuits, a higher PVCR is desired, which requires a high direct tunneling current with a concurrent low excess current. The magnitude of the current flowing through the diode is determined by both the PCD and the diode cross-sectional area. The PCD is mainly determined by the density of the available states at each δ-doped layer's quantum well, the intervening tunneling barrier composition, and its thickness. The δ-doping layers enable the degeneracy condition to be met for NDR and provide a well-defined localized region for carrier tunneling to occur between quantum wells. For a given material, the RITD's PCD was found to approximately increase exponentially with decreasing tunneling barrier thickness at the rate of $\sim 10^6 \exp(-0.6\ \mathrm{W})$.[12] Also, for Si/SiGe tunnel diodes, the authors previously found that by incorporating Ge into the tunneling barrier, for instance, by replacing a 4 nm tunneling barrier of pure i-Si with 2 nm i-Si and 2 nm of i-$Si_{0.5}Ge_{0.5}$, the tunneling current can be significantly increased from 3.1 to 22 $\mathrm{kA/cm^2}$.[8] This significant increase in current may not be due to barrier lowering from the alloy effect alone.

The design of a tunneling structure for phonon-assisted tunneling experiments is fundamentally the same as designing a high PVCR tunnel diode, both requiring a structure that facilitates tunneling while reducing as much as possible the excess current component due to crystal imperfections. The low-temperature nature of phonon-assisted tunneling experiments requires a structure with a low current in order to reduce Joule heating effects. This requires a low PCD and/or a small diode cross-sectional area. An added benefit of low PCD is that it also reduces the voltage drop across the metal-semiconductor contacts and the bulk resistances, which can become significant if too high. For a given tunneling barrier thickness, the incorporation of Ge in the tunneling barrier increases the PCD. However, the critical thickness for pseudomorphic $Si_{1-x}Ge_x$ layer on a Si substrate prevents a thick all-SiGe tunneling barrier layer, else misfit dislocations would greatly elevate the excess current by enhancing defect-related tunneling. The authors found that 4 nm is the upper limit for the $Si_{0.60}Ge_{0.40}$ layer in the tunneling barrier for high PVCR tunnel diodes using the growth procedure, which is described later. With diode mesa diameters ranging from 10 to 75 μm used in this experiment, the highest-PCD structure, corresponding to the thinnest total tunneling barrier thickness, consisted of 4 nm $Si_{0.60}Ge_{0.40}$ and 4 nm Si and did not appear to cause significant Joule heating during the low-temperature measurements.

The structures were grown by low-temperature molecular beam epitaxy (MBE) on 3 in. p^+-Si (100) substrates with a resistivity less than 0.005 Ω cm. The growth was initiated at a substrate temperature of 650 °C, which was lowered to 500 °C during the growth of the $5\times10^{19}\ \mathrm{cm^{-3}}$ p^+-Si with boron (B) as the dopant. Next, a 1 nm $p^+Si_{0.60}Ge_{0.40}$ layer was grown, followed by the growth of a B δ-doping plane with a sheet carrier concentration of $1\times10^{14}\ \mathrm{cm^{-2}}$ using the stop growth technique (i.e., the Si and Ge shutters were closed during the growth of the δ-doping layer). The substrate temperature was further lowered to 320 °C during the deposition of the B δ-doping plane, and this temperature was maintained for the rest of the growth. After the B δ-doping plane, the growth was resumed and 4 nm undoped $Si_{0.60}Ge_{0.40}$ and n nm undoped Si were grown. Then the stop growth technique was used again to deposit the phosphorus (P) δ-doping layer with a sheet concentration of $1\times10^{14}\ \mathrm{cm^{-2}}$, followed by the growth of 100 nm of $5\times10^{19}\ \mathrm{cm^{-3}}$ P-doped Si as the top contact layer, which completed the growth. A postgrowth rapid thermal annealing at 825 °C for 60 s in a 5% H_2/95% N_2 gas ambient was performed to reduce the density of defects in the crystal created during the low-temperature growth.[28,29] Devices with a circular mesa structure and two bonding pads were fabricated using photolithography and wet etching [Fig. 1(b)]. Plasma-enhanced chemical vapor deposited SiO_2 was used to provide a stable dielectric that was also patterned and etched to provide suitable electrically isolated bond pads. Portions of the fabricated wafers were then mounted on a 16-*pin* dual-in-line package, suitable for the low-temperature apparatus, and bonding wires connected the RITD electrodes to the package leads [Fig. 1(c)]. From each RITD structure, devices with various mesa diameters of 10, 18, 50, and 75 μm were fabricated and measured.

B. Measurement

The measurement system was based on the system developed by Feng *et al.* which measured dV/dI using the harmonic detection method,[30] i.e., applying a small-amplitude, high-quality single-frequency ac current and measuring the voltage signal at the first harmonic (the same frequency) with a lock-in amplifier. This instrument achieved an accuracy of better than 10^{-4} with modulation voltages as low as 50 μV and an overall thermal stability better than 10 ppm/°C. The

Downloaded 10 Aug 2009 to 164.107.166.49. Redistribution subject to AIP license or copyright; see http://jap.aip.org/jap/copyright.jsp

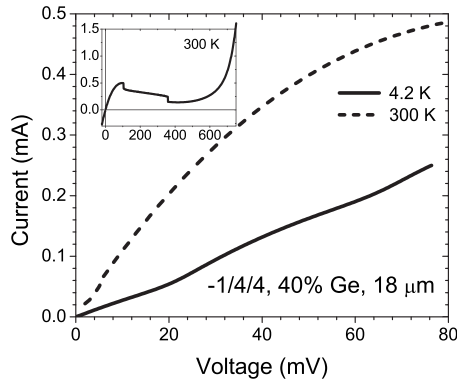

FIG. 2. *I-V* characteristics of a 18 μm diameter RITD using the $-1/4/4$ structure with $Si_{0.60}Ge_{0.40}$ measured at room temperature (300 K) and 4.2 K. Two weak inflections due to phonons are observable in the *I-V* curve measured at 4.2 K. The inset is the room-temperature *I-V* curve measured over a wider voltage range, displaying a negative-differential-resistance region which is characteristic of a tunnel diode.

modulation frequency used was $\sim$17 Hz. This instrument used the source-current-measure-voltage approach. The biasing current was provided by a high-precision biasing resistor and a voltage source, which was a 16-bit digital-to-analog converter controlled by a computer via an optical link (to prevent electric noise from the computer from entering the measuring circuit). The current sweep range was chosen so that for the diode being measured the biasing voltage varied between 0 and about 80 mV, sufficient to span the energy of the four primary phonons targeted for measurement. The current modulation amplitude was chosen so that the modulation voltage across the diode would not exceed 0.5 mV. About 200 data points were collected for each measured curve. At each current bias, the voltage and the first-order derivative dV/dI were measured and recorded. The derivative of dV/dI with respect to I, d^2V/dI^2, was then calculated using the three-point numerical differential formula, $df(x)/dx=[f(x+h)-f(x-h)]/(2h)+O(h^2)$. The second-order derivative of I with respect to V, d^2I/dV^2, was then obtained using these relationships,

$$\frac{dI}{dV} = \frac{1}{dV/dI}, \tag{1}$$

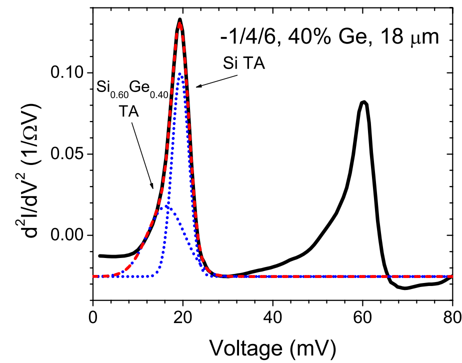

FIG. 4. (Color online) Measured phonon spectrum of an 18 μm RITD with the $-1/4/6$ $Si_{0.60}Ge_{0.40}$ structure and the Gaussian peak fit to the measured peak at $\sim$20 mV.

$$\frac{d^2I}{dV^2} = \frac{-1}{(dV/dI)^3}\frac{d^2V}{dI^2}. \tag{2}$$

Even though, in general, a directly measured d^2I/dV^2 versus V by the detection of the second harmonic (twice the modulation frequency) is preferred, our approach described above produced high quality low-noise d^2I/dV^2 data, as will be demonstrated. This was also confirmed by the excellent agreement between the measured Si phonon spectra using this method for commercial Si Esaki tunnel diodes and previously published data.[26]

III. RESULTS AND DISCUSSIONS

Representative *I-V* curves measured at room temperature (300 K) and 4.2 K are shown in Fig. 2. Weak inflections due to the onset of phonon participation in the tunneling process are present in the 4.2 K *I-V* curve. As shown in Figs. 3–6, the measured phonon spectra of the $-1/4/n$ $(n=4,6,8,10)$ structures were dominated by two major peaks at approximately 20 and 60 mV, related, respectively, to the strong TA and TO phonons of the Si and $Si_{0.60}Ge_{0.40}$ tunneling spacer, with slight voltage shifts due to a finite series resistance, which will be discussed later.

The peak at $\sim$20 mV is primarily due to the TA phonon of Si $[18.7\pm0.2$ meV (Ref. 26)] as the tunneling barriers contained Si layers of various thicknesses from 4 to 10 nm. The TA phonon of $Si_{0.60}Ge_{0.40}$ is most easily identified as the

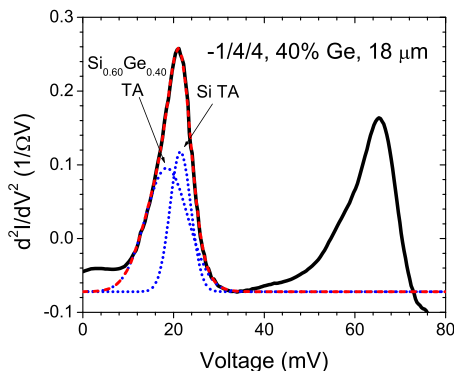

FIG. 3. (Color online) Measured phonon spectrum of an 18 μm RITD with the $-1/4/4$ $Si_{0.60}Ge_{0.40}$ structure and the Gaussian peak fit to the measured peak at $\sim$20 mV.

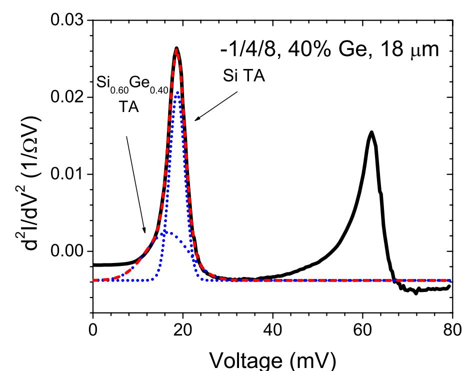

FIG. 5. (Color online) Measured phonon spectrum of an 18 μm RITD using the $-1/4/8$ $Si_{0.60}Ge_{0.40}$ structure and the Gaussian peak fit to the measured peak at $\sim$20 mV.

Downloaded 10 Aug 2009 to 164.107.166.49. Redistribution subject to AIP license or copyright; see http://jap.aip.org/jap/copyright.jsp

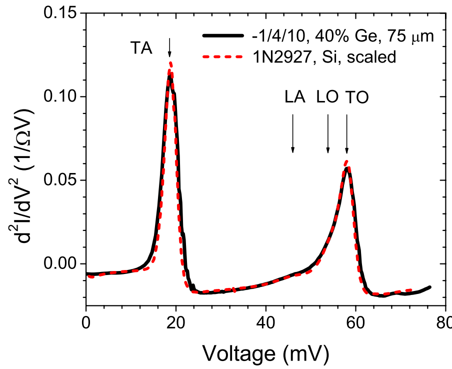

FIG. 6. (Color online) Measured phonon spectrum of an 18 μm RITD using the −1/4/10 $Si_{0.60}Ge_{0.40}$ structure and that of a commercial Si Esaki tunnel diode. The nearly complete overlap indicates that the measured phonon spectrum of the −1/4/10 RITD structure was almost completely dominated by the Si phonons. In addition, the agreement between the measured Si phonon spectrum and that reported by Logan *et al.* (Ref. 26) confirms the accuracy of the phonon spectra obtained in this experiment. Further, the −1/4/10 RITD structure did not suffer from appreciable voltage shift due to series resistance mainly because it exhibited the lowest current density of the RITDs measured in this experiment.

left shoulder of the ~20 mV peak in the phonon spectra, shown in Fig. 3, of the −1/4/4 structure, which had the highest weighted average of $Si_{0.60}Ge_{0.40}$ in the composite tunneling barrier among the RITD structures measured here. It should be noted that the tunneling spectroscopy technique used here will measure an ensemble of tunneling carriers, some of which interact with the Si layer and others the $Si_{0.60}Ge_{0.40}$ layer by tunneling into different virtual states spatially within the composite $Si/Si_{0.60}Ge_{0.40}$ tunneling spacer. This low-energy shoulder becomes progressively weaker as the structure moves from the −1/4/4 configuration to the −1/4/10 structure, as shown in Figs. 4–6, consistent with the decreasing weighted average of $Si_{0.60}Ge_{0.40}$ in the composite tunneling barrier. In fact, this shoulder is not identifiable in the phonon spectra (Fig. 6) of the −1/4/10 structure, which had the least weighted average of $Si_{0.60}Ge_{0.40}$ in the composite tunneling barrier.

Using the least-squares method, the peaks at ~20 mV with shoulders for the −1/4/4, −1/4/6, and −1/4/8 structures were fitted with two Gaussian peaks. The fit function is $f(x)=a_1\exp(-[(x-b_1)/c_1]^2)+a_2\exp(-[(x-b_2)/c_2]^2)+c_0$, where c_0 is a predetermined offset and a_1, b_1, c_1, a_2, b_2, and c_2 are fitting parameters. Parameters b_1 and b_2 correspond to the energies of each of the two convolved phonons, and a_1 and a_2 represent their relative magnitudes, respectively. The results of the fittings are shown in Figs. 3–5. The quality of the fittings is most evident in the plots by the almost complete overlap of the solid curve (measured data) and the long dashed curve (fitted curve) in the region of interest (i.e., the peak around 20 mV). The fittings are stable against small perturbations on the fitting region. It is concluded that the global minima in the least-squares space over the fitting regions are obtained in our fittings. The goodnesss of the peak fit is determined by the sum of squares due to error which is the summed square of residuals (difference between fitting and measured data). It is found to be 6.7×10^{-4}, 2.4×10^{-5}, and 2.73×10^{-6} for Figs. 3–5, respectively.

For a 18 μm diode of the −1/4/4 structure, the two fitted Gaussian peaks were located at 18.5 and 21.5 mV, with the height of the 18.5 mV peak assigned to a SiGe TA phonon being only slightly lower in magnitude (~88%) than that of the second peak, which could be a pure Si TA phonon. For the −1/4/6 and −1/4/8 structures, the heights of the lower-voltage peaks were ~35% and ~25%, respectively, of that of the higher-voltage peaks, considerably lower than those in the −1/4/4 structure (see Figs. 4 and 5). The fit results, including those for the 50 and 75 μm diodes, are listed in Table I. A similar shoulder could not be unambiguously identified in the phonon spectra obtained from the −1/4/10 structure (Fig. 6). Note that the weighted average of Si in the composite tunneling barrier increases and, correspondingly, that of $Si_{0.60}Ge_{0.40}$ decreases, as the sample structure varied from −1/4/4 to −1/4/10.

In fact, the measured phonon spectra of the −1/4/10 structure can hardly be differentiated from the phonon spectrum of pure Si measured from a commercial Si Esaki tunnel diode (Fig. 6). This is consistent with the expectation that since the −1/4/10 structure has the least weighted average of $Si_{0.60}Ge_{0.40}$ in the tunneling barrier, the Si phonon spectrum should dominate. It should be noted that there exists excellent agreement between the phonon spectra of the Si Esaki diode measured in this experiment, shown in Fig. 6, and that reported by Logan *et al.*[26] in terms of overall spectral shape and phonon peak locations which validates the high precision of the instruments and techniques used in this experiment (the higher resolution of the spectra obtained by Logan *et al.* was mainly due to less thermal broadening by using a much lower temperature of 0.8 K compared to 4.2 K used here). For instance, Logan *et al.*[26] reported the TA and TO peak positions for pure Si to be 18.7 ± 0.2 and 59.1 ± 0.2 mV, which are similar to the 18.9 and 58.2 mV extracted from the −1/4/10 sample.

The second, much wider, peak that appears at ~60 mV consists of the combination of weak and/or closely spaced LA, LO, and TO phonons of Si, and is superimposed with the corresponding phonons from the $Si_{0.60}Ge_{0.40}$ layer. The determination of the locations of these weaker and/or closely spaced phonons requires a higher sensitivity and higher resolution not yet achieved in this experiment. No attempt was made to resolve the $Si_{0.60}Ge_{0.40}$ LA, LO, and TO phonons by peak fitting.

For the measured peaks at ~20 meV, the fitted Si TA phonon peak location ranges from 18.7 to 23.0 meV, equal or higher than the previously reported value of 18.7 ± 0.2 meV. These are displayed in Fig. 7 as open triangles versus the current corresponding to the Si TA phonon peak. The fitted $Si_{0.60}Ge_{0.40}$ TA phonon peak locations, ranging from 16.2 to 21.9 meV, are shown in Fig. 7 as solid circles. The general trend of the upshift of both Si TA phonon and $Si_{0.60}Ge_{0.40}$ TA phonon peak locations with increasing current, as observed in Fig. 7, indicates that this shift was mainly due to series resistance of the sample. Accurate determination of phonon energies by electron tunneling spectroscopy requires a negligible voltage drop due to series resistance, or, in the presence of non-negligible series

Downloaded 10 Aug 2009 to 164.107.166.49. Redistribution subject to AIP license or copyright; see http://jap.aip.org/jap/copyright.jsp

TABLE I. Results of least-squares fit with two Gaussian peaks to the measured phonon peaks at ~20 mV for diodes of various structures and diameters. The fitting function is $f(x)=a_1\exp(-[(x-b_1)/c_1]^2)+a_2\exp(-[(x-b_2)/c_2]^2)+c_0$, where c_0 is a predetermined offset, and a_1, b_1, c_1, a_2, b_2, and c_2 are fitting parameters. The corresponding current at the Si TA phonon peak, which is related to the measured phonon peak shift due to series resistance, is listed in the last column.

	Fit						Current
	$Si_{0.60}Ge_{0.40}$ TA			Si TA			Si TA
RITD structure	a_1 (height) ($1/\Omega$V)	b_1 (center) (mV/meV)	c_1 (width) (mV)	a_2 (height) ($1/\Omega$V)	b_2 (center) (mV/meV)	c_2 (width) (mV)	$I(b_2)$ (mA)
−1/4/4							
18 μm diameter	0.1676	18.49	6.585	0.1900	21.52	3.257	0.059 3
50 μm diameter	1.470	19.58	6.903	1.787	21.90	2.743	0.575
75 μm diameter	3.042	21.75	7.690	2.583	22.97	2.880	1.13
−1/4/6							
18 μm diameter	0.043 19	16.22	5.828	0.1253	19.47	2.638	0.009 61
50 μm diameter	0.4132	16.76	5.500	1.177	19.59	2.085	0.084 5
75 μm diameter	0.9482	16.63	5.354	2.918	19.42	1.972	0.192
−1/4/8							
18 μm diameter	0.006 224	16.50	6.656	0.024 52	18.73	2.407	0.001 26
50 μm diameter	0.048 82	16.94	6.670	0.226 5	19.58	2.316	0.011 3
75 μm diameter	0.1693	16.70	5.518	0.651 9	18.93	1.992	0.026 9

resistance, must correct for the voltage drop due to series resistance, consisting of contact resistances and body resistances.

Attempt to correct the contact resistance in this experiment assuming current-independent Ohmic contacts failed to yield consistent results, indicating that the *I-V* characteristics of at least one of the two metal-Si contacts in the tunneling junction were nonlinear, and the Ohmic contacts obtained in this experiment were nonoptimal. Optimizing the Ohmic contacts is required for future experiments. On the other hand, under certain conditions, reducing the current flow can alleviate the problem of series resistance by reducing the voltage drop due to the series resistance. The trend shown in Fig. 7 indicates that this was the case in this experiment. This

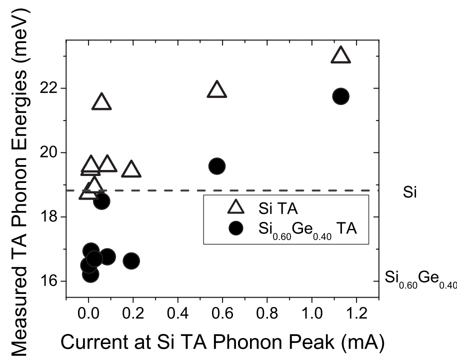

FIG. 7. Scatter plot of fitted Si TA phonon energy (solid circles) and $Si_{0.60}Ge_{0.40}$ TA phonon energy (open triangles) vs current at the Si TA phonon peak. Upshift of phonon energies due to contact resistance is shown. The convergence of both Si TA phonon and $Si_{0.60}Ge_{0.40}$ TA phonon energies at low current levels indicates that the effect of contact resistance was negligible at these current levels. The agreement of measured low current Si TA phonon energy with previously reported data leads to a determination of about 16 meV for the $Si_{0.60}Ge_{0.40}$ TA phonon energy in this experiment.

is further confirmed by the fact that the −1/4/10 structure, having the lowest current density, was the least affected by series resistance, as can be seen in Fig. 6.

Without series resistance correction due to the lack of full knowledge on the contacts' *I-V* characteristics and the body resistance, the convergence of the data points toward lower currents in Fig. 7 indicates that the effect of series resistance was negligible at such low current levels. At these low current levels, the known Si TA phonon energy was measured to be at, or slightly higher than, 18.7 meV, in agreement with the previously reported values and it served as a source of calibration. At the same current levels, the $Si_{0.60}Ge_{0.40}$ TA phonon energy was measured, however, to be slightly higher than 16.0 meV. Observing that there is still a slight unaccounted upshift of the Si TA phonon energy as compared to the previously reported value, which may come from the tensial stress of the Si in contact with the $Si_{0.60}Ge_{0.40}$. We conclude that the $Si_{0.60}Ge_{0.40}$ TA phonon energy as measured in this experiment was about 16 meV.

The experimentally measured peaks in d^2I/dV^2 versus V are widened from their intrinsic widths by thermal broadening due to the finite measurement temperature (4.2 K) and modulation broadening due to finite modulation voltage. The total full width at half maximum (FWHM) due to thermal broadening and modulation broadening is given by

$$\text{FWHM} = \sqrt{(5.4k_BT)^2 + (1.2eV_\omega)^2}, \quad (3)$$

where k_B is the Boltzmann constant, T is the absolute temperature in K, e is the electron charge, and V_ω is the modulation amplitude.[31,32] At 4.2 K, $k_BT=1.95$ meV. Typically the modulation amplitude is chosen so that modulation broadening is comparable to thermal broadening. Even though, in general, the peak width and peak location are two indepen-

Downloaded 10 Aug 2009 to 164.107.166.49. Redistribution subject to AIP license or copyright; see http://jap.aip.org/jap/copyright.jsp

dent parameters, the resolution of the phonon energy, or peak location, measurement is affected by peak broadening effects. In this experiment, only the phonon peak locations, i.e., phonon energies, were measured, and the peak widths were not measured. The error in phonon energy measurement in this experiment is estimated to be ±1 mV. Note that the resolution can be improved by using a temperature lower than 4.2 K and a correspondingly lower modulation amplitude. Notice, however, with a lower modulation amplitude, the time constant of the lock-in amplifier needs to be increased in order to achieve a good signal-to-noise ratio, which usually results in significantly increased measurement times that would greatly elevate the measurement's sensitivity to environmental noise.

For comparison, Logan *et al.* measured the phonon energies of bulk $Si_{1-x}Ge_x$ at a number of discrete compositions ranging from pure Si to pure Ge using an Esaki tunnel diode structure.[26] Their measurements utilized a second derivative analysis of tunneling Esaki diodes, sharing basic similarities to the technique explored here. Interpolation of their $Si_{1-x}Ge_x$ data gives an estimated energy of ~14 meV for the TA phonon of bulk $Si_{0.60}Ge_{0.40}$. The $Si_{0.60}Ge_{0.40}$ TA phonon energy obtained in this experiment using pseudomorphic $Si_{0.60}Ge_{0.40}$ is about 16±1 meV. According to Logan *et al.*,[26] a TA phonon energy of 16 meV corresponds to an unstrained SiGe alloy with about 20% Ge. Since the Esaki tunnel diodes were made in bulk single crystals, we attribute the 2±1 meV increase in the extracted TA phonon energy of the $Si_{0.60}Ge_{0.40}$ layers in the Si/SiGe RITDs grown on Si substrates to the compressive strain that is residual in the $Si_{0.60}Ge_{0.40}$ layers contained within the composite tunneling spacer.

For further comparison, Tsang *et al.* measured the composition and strain of thin $Si_{1-x}Ge_x$ layers grown on Si substrates for $0 \leq x \leq 0.5$ using Raman spectroscopy.[22] It should be noted that Raman spectroscopy probes the optical phonons, which are at higher energies and not the TA phonon analyzed here, but may serve as a guidepost. Nevertheless, the frequencies of the Si–Si and the Ge–Si peaks in their Raman spectra were determined to be, respectively,

$$\omega_{Si} = 520.0 - 68x + 34\Sigma \ (\mathrm{cm}^{-1}), \tag{4}$$

$$\omega_{GS} = 400.5 + 14.2x + 24\Sigma \ (\mathrm{cm}^{-1}), \tag{5}$$

where x is the Ge concentration and $\Sigma = -(a-a_0)/a_0$ $(1/0.0417)$ is the strain normalized to the compressive strain of pseudomorphic Ge grown on Si substrate, and a and a_0 are the strained and relaxed lattice constants of $Si_{1-x}Ge_x$ alloys, respectively. The lattice constant of bulk $Si_{1-x}Ge_x$ alloy is slightly lower than the linear interpolation between the Si and the Ge lattice constants, $a_0 = 5.5149$ Å for $Si_{0.60}Ge_{0.40}$.[33] Assuming that the $Si_{1-x}Ge_x$ layers grown on a Si substrate in this experiment are completely strained, i.e., pseudomorphic, the strained lattice parameter in the plane of growth is that of bulk Si, i.e., $a = 5.431$ Å. The normalized compressive strain is therefore $\Sigma = (5.515 - 5.431)/(5.515)\ (1/0.0417) = 0.3653$. For $x = 0.40$, the change in the Si–Si and Ge–Si optical phonon peak frequencies are $34\Sigma = +12.4\ \mathrm{cm}^{-1}$ and $24\Sigma = +8.8\ \mathrm{cm}^{-1}$, respectively. These frequency changes correspond to energy changes of +1.54 and +1.09 meV, respectively. The magnitude is comparable to the +2 meV change to the TA phonon energy (of approximately 14 meV) obtained in this experiment, although it must be pointed out that the above calculations are for the change in the energy of optical phonons measured by Raman spectroscopy in the range around 50 meV.

The observation of this upshift of the $Si_{0.60}Ge_{0.40}$ TA phonon energy by strain with electron tunneling spectroscopy, as shown in this experiment, demonstrates the capability of electron tunneling spectroscopy to characterize the strain in thin pseudomorphic layers. It is reasonable to expect that, once properly calibrated with XRD and/or Raman spectroscopy, the shift in the phonon energy measured by electron tunneling spectroscopy could be used to quantitatively characterize the strain. One advantage of electron tunneling spectroscopy is that it offers the possibility of characterizing buried layers where XRD and Raman spectroscopy may have difficulty.

It should be noted that in these δ-doped RITDs, the Si phonons dominate the extracted spectra for the Si/SiGe RITDs with only a lesser participation of SiGe phonons. For example, the approximate ratios of the measured magnitude of the SiGe TA phonon compared to the Si TA phonon are ~88%, ~35%, and ~25%, respectively, for the −1/4/4, −1/4/6, and −1/4/8 composite tunneling spacers. Following the weighted average of SiGe leads to an expected ratio of SiGe versus Si TA phonons of 100%, 67%, and 50%, in contrast to the extracted results. The discrepancy may reveal some internal physics not fully discussed previously for Si-based RITDs.

Indeed, it has long been recognized that the addition of Ge to the central tunneling region of RITDs increases the measured current density significantly[8,10,11] as well as the RITD's thermal budget.[9] The Ge-containing layers serve a vital role by surrounding the B δ-doped spike acting as dopant diffusion barriers, thereby facilitating higher annealing temperatures for better point defect annihilation without B outdiffusion from the δ-doped spike.[9] Principally, these point defects are vacancies created by the low substrate temperature during MBE growth,[28] which is needed to suppress Ge, P, and B segregation during growth and *in situ* diffusion. The reduced substrate temperature limits the ability of surface adatoms to move in a correlated manner to a step edge, creating vacancy-type defects.[28,29]

The addition of increasing amounts of Ge to the central spacer certainly lowers the tunneling barrier as the effective composite bandgap E_g of the RITD tunneling spacer reduces and also shrinks the effective mass m^*, thereby greatly increasing the tunneling probability and associated tunneling current density, as shown in Eq. (6) below from Kane's model,[34,35]

$$J_t \propto \frac{q^2 \varepsilon}{36\pi\hbar^2}\sqrt{\frac{2m^*}{E_g}}\exp\left(-\frac{4\sqrt{2m^*}E_g^{3/2}}{3q\hbar\varepsilon}\right). \tag{6}$$

Equation (6) indicates the major contributors to the band-to-band tunneling transmission through a triangular potential barrier, neglecting the overlap integral D as a function of

Downloaded 10 Aug 2009 to 164.107.166.49. Redistribution subject to AIP license or copyright; see http://jap.aip.org/jap/copyright.jsp

external bias since only the PCD is relevant here. $\mathcal{E}$ is the average electric field housed within these ultranarrow junctions, often of the order of 10^6 V/cm, assuming the bandgap voltage is distributed across a 2–10 nm tunneling spacer. However, the significant rise in the recorded PCD, as mentioned earlier, may not be accounted for fully by the weighted average of the smaller bandgap Ge.

The influence of strain, whether compressive or tensile, is known to reduce bandgap,[13] and the nanoscale proximity of the narrow active RITD tunneling barrier to the Si/SiGe interface must encompass this effect and further amplify the increase in tunneling probability. Indeed, similar observations were made with the enhanced mobility of Si/SiGe modulation doped field effect transistors, where the channel resides at the Si/SiGe interface.[36,37]

The highly localized δ-doping used in these RITDs may also provide a mechanism for momentum mixing by the distributed states in k-space, and thereby also contribute to the large recorded current densities in prior δ-doped RITDs,[10,11] but this requires further study. Lastly, previous full band modeling of the phonon participation in RITDs using a nonequilibrium Green's function formalism with a second-neighbor sp^3s^* planar orbital basis focused solely on Si-only RITDs.[38,39] These experimental results should provide a guidepost to future modeling of Si/SiGe RITDs and other Si/SiGe heterostructure band-to-band tunneling.

IV. CONCLUSIONS

To summarize, electron tunneling spectroscopy was used to measure the phonon spectra in the Si/SiGe RITDs. With composite tunneling barriers consisting of 4 nm intrinsic $Si_{0.60}Ge_{0.40}$ and n nm of intrinsic Si ($n=4,6,8,10$) grown on Si substrates, the TA phonon of $Si_{0.60}Ge_{0.40}$ was identified and the energy was measured to be 16 ± 1 meV. This is higher than the ~14 meV energy of $Si_{0.60}Ge_{0.40}$ from measurements using Esaki tunnel diodes made of bulk single crystals. The increase is attributed to the compressive strain in the $Si_{0.60}Ge_{0.40}$ layer grown on a Si substrate. The observation of strain by electron tunneling spectroscopy demonstrates the capability of electron tunneling spectroscopy to characterize strain. Electron tunneling spectroscopy can be a useful technique for strain characterization, complementing the existing techniques of XRD and Raman scattering, and especially offering the advantage of being able to characterize buried layers.

ACKNOWLEDGMENTS

This work at OSU was partially supported by the NSF (Grant No. DMR-0103248). The work at NRL was supported by ONR. R.Y. would like to acknowledge the support provided by the OSU Physics Department. In fond memory of Ralph A. Logan, a former Bell Labs colleague (PRB), who sadly left us December 2006.

[1] P. van der Wagt, A. Seabaugh, and E. Beam III, Tech. Dig. - Int. Electron Devices Meet. **1996**, 425.
[2] T. P. E. Broekaert, B. Brar, J. P. A. van der Wagt, A. C. Seabaugh, F. J. Morris, T. S. Moise, E. A. Beam III, and G. A. Frazier, IEEE J. Solid-State Circuits **33**, 1342 (1998).
[3] H. J. De Los Santos, K. K. Chui, D. H. Chow, and H. L. Dunlap, IEEE Microw. Wirel. Compon. Lett. **11**, 193 (2001).
[4] A. Cidronali, G. Collodi, M. Camprini, V. Nair, G. Manes, J. Lewis, and H. Goronkin, *IEEE RFIC Symposium 2002* (unpublished), p. 297.
[5] The International Technology Roadmap for Semiconductors (ITRS) (http://www.itrs.net/).
[6] S. L. Rommel, T. E. Dillon, M. W. Dashiell, H. Feng, J. Kolodzey, P. R. Berger, P. E. Thompson, K. D. Hobart, R. Lake, A. C. Seabaugh, G. Klimeck, and D. K. Blanks, Appl. Phys. Lett. **73**, 2191 (1998).
[7] S. L. Rommel, T. E. Dillon, P. R. Berger, P. E. Thompson, K. D. Hobart, R. Lake, and A. C. Seabaugh, IEEE Electron Device Lett. **20**, 329 (1999).
[8] S. L. Rommel, T. E. Dillon, P. R. Berger, R. Lake, P. E. Thompson, K. D. Hobart, A. C. Seabaugh, and D. S. Simons, Tech. Dig. - Int. Electron Devices Meet. **1998**, 1035.
[9] N. Jin, S.-Y. Chung, A. T. Rice, P. R. Berger, P. E. Thompson, C. Rivas, R. Lake, S. Sudirgo, J. J. Kempisty, B. Curanovic, S. L. Rommel, K. D. Hirschman, S. K. Kurinec, P. H. Chi, and D. S. Simons, IEEE Trans. Electron Devices **50**, 1876 (2003).
[10] N. Jin, S.-Y. Chung, A. T. Rice, P. R. Berger, R. Yu, P. E. Thompson, and R. Lake, Appl. Phys. Lett. **83**, 3308 (2003).
[11] S.-Y. Chung, R. Yu, N. Jin, S.-Y. Park, P. R. Berger, and P. E. Thompson, IEEE Electron Device Lett. **27**, 364 (2006).
[12] N. Jin, S.-Y. Chung, R. Yu, R. M. Heyns, P. R. Berger, and P. E. Thompson, IEEE Trans. Electron Devices **53**, 2243 (2006).
[13] *Properties of Silicon Germanium and SiGe:Carbon*, edited by Erich Kasper and Klara Lyutovich (INSPEC, London, 2000).
[14] M. V. Fischetti and S. E. Laux, J. Appl. Phys. **80**, 2234 (1996).
[15] J. Welser, J. L. Hoyt, and J. F. Gibbons, Tech. Dig. - Int. Electron Devices Meet. **1992**, 1000.
[16] M. L. Lee, E. A. Fitzgerald, M. T. Bulsara, M. T. Currie, and A. Lochtefeld, J. Appl. Phys. **97**, 011101 (2005).
[17] J. Hornstra and W. J. Bartels, J. Cryst. Growth **44**, 513 (1978).
[18] W. J. Bartels and W. Nijman, J. Cryst. Growth **44**, 518 (1978).
[19] M. Fatemi and R. E. Stahlbush, Appl. Phys. Lett. **58**, 825 (1991).
[20] M. A. Renucci, J. B. Renucci, and M. Cardona, in *Light Scattering in Solids*, edited by M. Balkanski (Flammarion Sciences, Paris, 1971), pp. 326–329.
[21] F. Cerdeira, A. Pinczuk, J. C. Bean, B. Batlogg, and B. A. Wilson, Appl. Phys. Lett. **45**, 1138 (1984).
[22] J. C. Tsang, P. M. Mooney, F. Dacol, and J. O. Chu, J. Appl. Phys. **75**, 8098 (1994).
[23] N. Holonyak Jr., I. A. Lesk, R. N. Hall, J. J. Tiemann, and H. Ehrenreich, Phys. Rev. Lett. **3**, 167 (1959).
[24] A. G. Chynoweth, R. A. Logan, and D. E. Thomas, Phys. Rev. **125**, 877 (1962).
[25] R. T. Payne, Phys. Rev. **139**, A570 (1965).
[26] R. A. Logan, J. M. Rowell, and F. A. Trumbore, Phys. Rev. **136**, A1751 (1964).
[27] R. People and J. C. Bean, Appl. Phys. Lett. **47**, 322 (1985).
[28] S.-Y. Chung, N. Jin, A. T. Rice, P. R. Berger, R. Yu, Z.-Q. Fang, and P. E. Thompson, J. Appl. Phys. **93**, 9104 (2003).
[29] S.-Y. Chung, N. Jin, R. E. Pavlovicz, P. R. Berger, R. Yu, Z.-Q. Fang, and P. E. Thompson, J. Appl. Phys. **96**, 747 (2004).
[30] X. G. Feng, S. Zelakiewicz, and T. J. Gramila, Rev. Sci. Instrum. **70**, 2365 (1999).
[31] J. Lambe and R. C. Jaklevic, Phys. Rev. **165**, 821 (1968).
[32] J. Klein, A. Leger, M. Belin, D. Defourneau, and M. J. L. Sangster, Phys. Rev. B **7**, 2336 (1973).
[33] J. P. Dismukes, L. Ekstrom, and R. J. Paff, J. Phys. Chem. **68**, 3021 (1964).
[34] E. O. Kane, J. Appl. Phys. **32**, 83 (1961).
[35] S. M. Sze and K. K. Ng, *Physics of Semiconductor Devices*, 3rd ed. (Wiley, New York, 2007).
[36] H. Daembkes, H.-J. Herzog, H. Jorke, H. Kibbel, and E. Kasper, IEEE Trans. Electron Devices **33**, 633 (1986).
[37] K. Ismail, B. S. Meyerson, S. Rishton, J. Chu, S. Nelson, and J. Nocera, IEEE Electron Device Lett. **13**, 229 (1992).
[38] C. Rivas, R. Lake, G. Klimeck, W. R. Frensley, M. V. Fishetti, P. E. Thompson, S. L. Rommel, and P. R. Berger, Appl. Phys. Lett. **78**, 814 (2001).
[39] C. Rivas, R. Lake, W. R. Frensley, G. Klimeck, P. E. Thompson, K. D. Hobart, S. L. Rommel, and P. R. Berger, J. Appl. Phys. **94**, 5005 (2003).

Downloaded 10 Aug 2009 to 164.107.166.49. Redistribution subject to AIP license or copyright; see http://jap.aip.org/jap/copyright.jsp